PNAS RESEARCH ARTICLE | CELL BIOLOGY

UBR2 targets myosin heavy chain IIb and IIx for degradation: Molecular mechanism essential for cancer-induced muscle wasting

Song Gao[a], Guohua Zhang[a,1], Zicheng Zhang[a], James Z. Zhu[a], Li Li[a], Yong Zhou[a], George G. Rodney Jr.[b], Reem S. Abo-Zahrah[b], Lindsey Anderson[c,d], Jose M. Garcia[c,d], Yong Tae Kwon[e], and Yi-Ping Li[a,2]

Edited by Se-Jin Lee, University of Connecticut School of Medicine, Farmington, CT; received January 7, 2022; accepted August 6, 2022

Cancer cachexia is a lethal metabolic syndrome featuring muscle wasting with preferential loss of fast-twitching muscle mass through an undefined mechanism. Here, we show that cancer induces muscle wasting by selectively degrading myosin heavy chain (MHC) subtypes IIb and IIx through E3 ligase UBR2-mediated ubiquitylation. Induction of MHC loss and atrophy in C2C12 myotubes and mouse tibialis anterior (TA) by murine cancer cells required UBR2 up-regulation by cancer. Genetic gain or loss of UBR2 function inversely altered MHC level and muscle mass in TA of tumor-free mice. UBR2 selectively interacted with and ubiquitylated MHC-IIb and MHC-IIx through its substrate recognition and catalytic domain, respectively, in C2C12 myotubes. Elevation of UBR2 in muscle of tumor-bearing or free mice caused loss of MHC-IIb and MHC-IIx but not MHC-I and MHC-IIa or other myofibrillar proteins, including α-actin, troponin, tropomyosin, and tropomodulin. Muscle-specific knockout of UBR2 spared KPC tumor-bearing mice from losing MHC-IIb and MHC-IIx, fast-twitching muscle mass, cross-sectional area, and contractile force. The rectus abdominis (RA) muscle of patients with cachexia-prone cancers displayed a selective reduction of MHC-IIx in correlation with higher UBR2 levels. These data suggest that UBR2 is a regulator of MHC-IIb/IIx essential for cancer-induced muscle wasting, and that therapeutic interventions can be designed by blocking UBR2 up-regulation by cancer.

cancer cachexia | UBR2 | ubiquitylation | MHC-IIb | MHC-IIx

Cachexia is a lethal metabolic disorder seen in ∼60% of cancer patients. The primary manifestation of cachexia is muscle wasting resulting in progressive loss of muscle mass and function. Cancer cachexia not only impairs patients' body metabolism and physical capacity, but also increases the toxicity and decreases the efficacy of chemotherapy, contributing significantly to cancer-associated morbidity and mortality (1, 2). However, the detailed mechanism through which cancer causes muscle wasting remains undefined. A distinctive feature of murine cancer cachexia is that the loss of muscle mass takes place preferentially in the fast-twitching muscles (3), in contrast to muscle atrophy due to denervation or disuse where the loss of muscle mass takes place primarily in the slow-twitching muscles (4). Given that myosin is by far the major contractile protein in skeletal muscle, the selective loss of fast-twitching muscles may result from the high susceptibility of fast myosin heavy chain (MHC) to degradation induced by catabolic mediators that are elevated in the cancer milieu (5). However, how cancer causes preferential loss of fast MHC is unknown, which hinders the understanding of the pathogenesis and the treatment of cancer cachexia.

Degradation of myofibrillar proteins, including myosin, is mediated by the ubiquitin-proteasome pathway (UPP), in which E3 ligases attach a polyubiquitin chain to specific substrate proteins to mark them for degradation by the 26S proteasomes (6). Four MHC isoforms are present in mouse skeletal muscle: I (slow and oxidative myofibers), IIa (fast and oxidative myofibers), and IIb and IIx (fast and glycolytic myofibers) (7). The E3 ligase MuRF1 ubiquitylates MHC, including β/slow MHC in cardiac muscle and MHC-IIa in skeletal muscle (8). In addition, MuRF1 ubiquitylates other thick filament components, including myosin-binding protein C and myosin light chains 1 and 2 in muscle atrophy induced by denervation (9). MuRF1 also mediates dexamethasone-induced degradation of MHC (10) and α-actin (11). However, the E3 that targets MHC IIb and IIx present in fast-twitching myofibers for degradation has not been identified. Thus, identifying the E3 responsible for the degradation of fast MHC, particularly during cancer cachexia, is not only important for skeletal muscle physiology but also for the understanding of the pathogenesis of cancer-associated muscle wasting. The current study is aimed at addressing this gap in our knowledge.

Significance

The preferential loss of fast-twitching muscle mass during cancer-induced muscle wasting is mediated by the ubiquitin-proteasome pathway; however, the detailed mechanism is unknown. We demonstrate that E3 ligase UBR2 selectively ubiquitylates myosin heavy chain (MHC) subtype IIb and IIx in fast-twitching muscle for degradation, but not MHC subtype I and IIa in slow-twitching muscle, as well as other myofibrillar proteins including α-actin, troponin, tropomyosin, and tropomodulin. UBR2 up-regulation is necessary and sufficient for the loss of fast-twitching muscle mass and contractile function in tumor-bearing mice. Patients with cachexia-prone cancers display a selective reduction of MHC-IIx in correlation with an elevation of UBR2 in skeletal muscle. Thus, UBR2 is a physiological and pathological regulator of MHC-IIb/IIx critical for cancer-induced muscle wasting.

The authors declare no competing interest.

This article is a PNAS Direct Submission.

[1]Present address: Gaoxin Hospital of the First Affiliated Hospital of Nanchang University, Nanchang, Jiangxi, 330046, China.

[2]To whom correspondence may be addressed. Email: yi-ping.li@uth.tmc.edu.

This article contains supporting information online at http://www.pnas.org/lookup/suppl/doi:10.1073/pnas.2200215119/-/DCSupplemental.

Published October 17, 2022.

Activity of the N-end rule pathway is responsible for a large portion of total protein ubiquitylation in myocytes induced by such inflammatory conditions as sepsis, cancer, and diabetes (12–14). MAFbx (also known as atrogin-1) and MuRF1 are two extensively studied E3 ligases important for muscle atrophy (15, 16). However, they do not belong to the N-end rule pathway. On the other hand, UBR2 (also known as E3α-II) is an E3 ligase highly expressed in skeletal muscle and serves as the substrate recognition component of the N-end rule pathway (17, 18). UBR2 is up-regulated in skeletal muscle of mice bearing cachexia-inducing cancers, including C26 colon adenocarcinoma, YAH-130 hepatoma, Lewis lung carcinoma (LLC), and $Apc^{min/+}$ mutation–induced intestine adenocarcinoma (18–21) as well as humans with gastrointestinal (GI) or genitourinary (GU) cancers (22, 23). Cancer up-regulates UBR2 through the p38β MAPK–C/EBPβ signaling pathway (21) that is critical for cancer-induced muscle wasting (24–26). These data suggest a potential involvement of UBR2 in cancer-induced muscle wasting. However, the substrate(s) of UBR2 in skeletal muscle has not been identified. In the present study we demonstrate that UBR2 mediates the ubiquitylation and degradation of MHC IIb and IIx in fast-twitching muscles of cancer-bearing as well as cancer-free mice. UBR2 up-regulation is necessary and sufficient for cancer-induced loss of muscle mass and contractile force. In addition, higher UBR2 levels detected in the rectus abdominis (RA) muscle of patients with cachexia-prone cancers correlate with a selective loss of MHC IIx. These data suggest that UBR2 is a physiological and pathological regulator of MHC degradation in fast-twitching muscles essential for cancer-induced muscle wasting.

Results

Up-Regulation of UBR2 in C2C12 Myotubes Is Required for MHC Loss and Myotube Atrophy Induced by Cancer Cell–Released Catabolic Factors. C2C12 myotubes are susceptible to atrophy upon exposure to the catabolic mediators present in the cancer milieu, including inflammatory cytokines and Hsp70/90 (5, 19, 26–28). To evaluate the selective targeting of myofibrillar proteins for degradation by cachectic cancer cells, we first compared total MHC and α-actin levels in C2C12 myotubes treated with conditioned medium of diverse types of cachectic cancer cells, including murine LLC and C26, as well as human H1299 lung carcinoma and BxPC3 pancreatic ductal adenocarcinoma, controlled with conditioned medium of nontumorigenic human lung epithelial cell NL20 (19). All cancer cell–conditioned media caused more than 40% loss of MHC in C2C12 myotubes in 72 h without altering α-actin content, suggesting that diverse types of cachexia-inducing cancer cells induce MHC loss in C2C12 myotubes in a discriminative manner (Fig. 1*A*). Due to the known role of MuRF1 in degrading MHC in slow-twitching muscle (8–10) and α-actin (11), we compared UBR2 and MuRF1 expression in the myotubes and observed UBR2 up-regulation in response to all of the cancer cell–conditioned media prior to MHC loss at 8 h, but MuRF1 level remained unaltered (Fig. 1*B*). We previously observed that the *MuRF1* mRNA is not increased in myotubes treated with LLC cell–conditioned medium and tibialis anterior (TA) of LLC tumor–bearing mice (26). We further observed here that the *MuRF1* mRNA was not increased in myotubes treated with C26 cell–conditioned medium for 8 h (*SI Appendix*, Fig. S1), confirming that MuRF1 expression is not up-regulated by catabolic factors released by these cancer cells. In contrast, consistent with the protein data, the *UBR2* mRNA was shown previously up-regulated by LLC cell–conditioned medium in myotubes (21). In addition, UBR2, but not α-actin, was up-regulated, leading to MHC loss in C2C12 myotubes treated with conditioned medium of mouse pancreatic ductal adenocarcinoma KPC cells (*SI Appendix*, Fig. S2) derived from the original KPC mice with pancreatic-specific, conditional alleles of the $KRAS^{G12D}$ and $TP53^{R172H}$ mutations (29) through backcrossing to the C57BL/6 background (30), which consistently induce cachexia in mice (25, 31). Because Hsp70 and Hsp90 are key components in cancer cell–conditioned media that cause muscle wasting (32), we verified that recombinant Hsp70 and Hsp90 treatment of myotubes up-regulated UBR2 but not MuRF1 (Fig. 1*C*). To determine whether UBR2 or MuRF1 is required for cancer cell–conditioned medium-induced MHC loss, their expression in myotubes was knocked down by specific siRNA and verified by Western blotting. Knockdown of UBR2 (Fig. 1 *D* and *E*), but not MuRF1 (Fig. 1 *F* and *G*), abrogated MHC loss and myotube atrophy induced by conditioned medium of LLC (LCM) or C26 (CCM). Further, overexpression of a dominant-negative mutant of UBR2 (DN-UBR2) that carried point mutations in its catalytic domain (17) in C2C12 myotubes abrogated MHC loss induced by the conditioned media (Fig. 1*H*). Moreover, overexpression of DN-UBR2 abrogated MHC loss induced by recombinant Hsp70 and Hsp90 in myotubes (Fig. 1*I*). These results indicate that UBR2, in contrast to MuRF1, is prevalently up-regulated by catabolic factors released by diverse types of cachectic cancer cells and is essential for the ensuing MHC loss and myotube atrophy.

UBR2 Is Critical for Loss of MHC and Mass of Fast-Twitching Muscles in Tumor-Bearing Mice. To examine whether UBR2 is required for cancer-induced loss of MHC and mass in fast-twitching muscles, DN-UBR2 with FLAG tag was overexpressed in the TA of LLC tumor–bearing male mice, which attenuated the loss of MHC (Fig. 2*A*), muscle weight (Fig. 2*B*), and myofiber cross-sectional area (Fig. 2*C*) or minimum Feret diameter (*SI Appendix*, Fig. S3*A*) of DN-UBR2–positive fibers. Similarly, overexpression of DN-UBR2 in the TA of KPC tumor–bearing male mice attenuated the loss of MHC (*SI Appendix*, Fig. S4). These data indicate that UBR2 is required for the loss of MHC and mass of fast-twitching muscles in mice bearing diverse types of cachexia-inducing tumors.

UBR2 Is a Physiological Regulator of MHC and Mass of Fast-Twitching Muscles. Skeletal muscle constitutively expresses UBR2 (17), suggesting a physiological role for this E3 in muscle mass homeostasis. To assess whether UBR2 regulates MHC and mass of fast-twitching muscles independent of tumors, wild-type UBR2 (WT-UBR2) was overexpressed in the TA of cancer-free male mice, which resulted in a loss of MHC (Fig. 3*A*), TA weight (Fig. 3*B*), myofiber cross-sectional area (Fig. 3*C*), and minimum Feret diameter (*SI Appendix*, Fig. S3*B*) of WT-UBR2–transfected fibers. Conversely, overexpression of DN-UBR2 in the TA of cancer-free male mice resulted in an increase in MHC content (Fig. 3*D*), TA weight (Fig. 3*E*), myofiber cross-sectional area (Fig. 3*F*), and minimum Feret diameter (*SI Appendix*, Fig. S3*C*) of DN-UBR2–transfected fibers. These data indicate an inverse relationship between UBR2 level/activity and MHC content/mass of fast-twitching muscles, suggesting that UBR2 is a physiological regulator of MHC turnover and mass of fast-twitching muscles.

UBR2 Selectively Ubiquitylates MHC IIb and IIx for Proteasomal Degradation in C2C12 Myotubes. To determine whether UBR2 is responsible for the ubiquitylation of MHC in

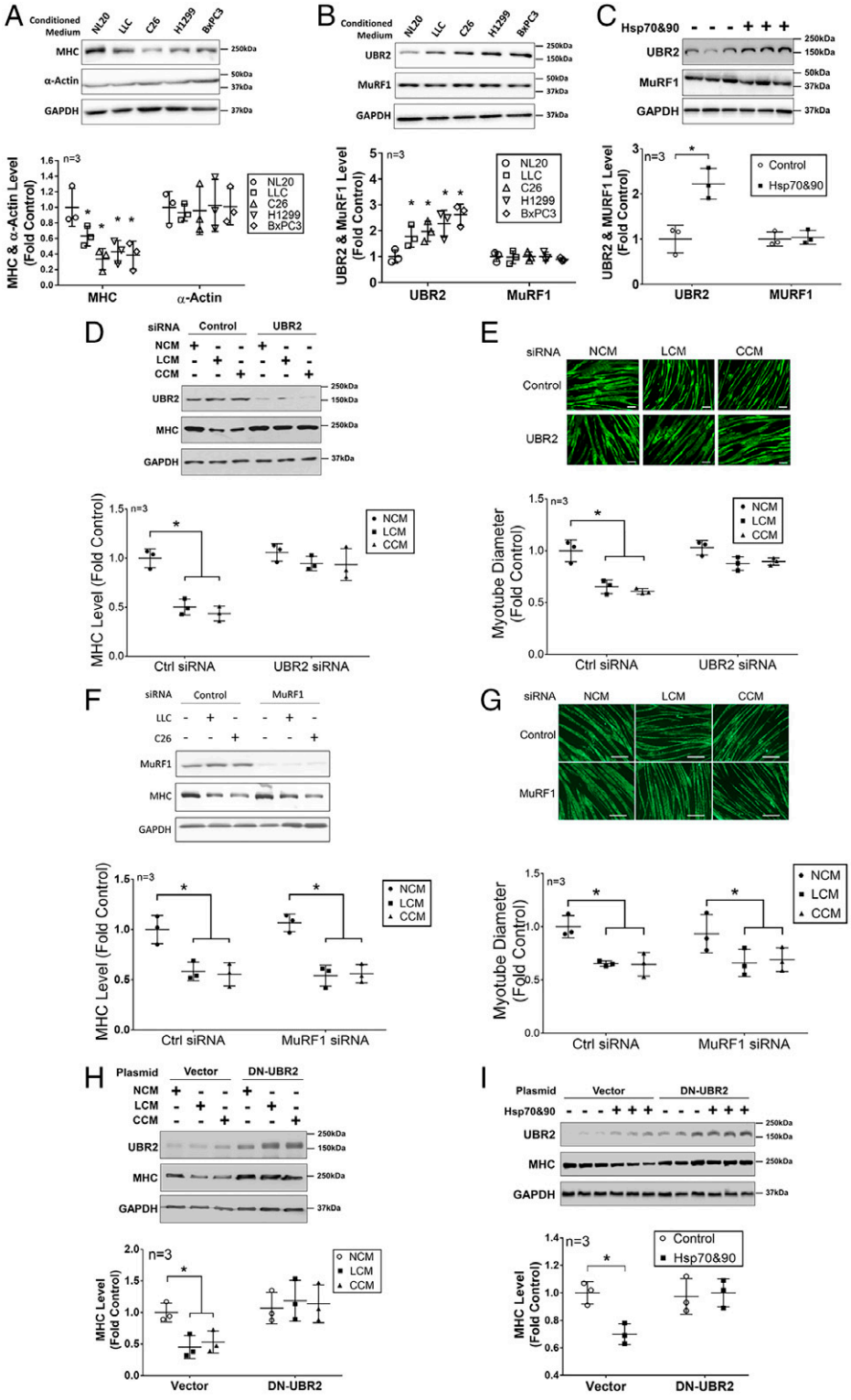

Fig. 1. UBR2 is critical for MHC loss and atrophy in C2C12 myotubes induced by cancer cell–conditioned media. (*A*) Cachectic cancer cell–conditioned media induce MHC loss without affecting α-actin. Myotubes were treated with conditional medium of LLC, C26, H1299, or BxPC3 cancer cells (controlled by nontumorigenic human lung epithelial cell NL20) for 72 h. Content of total MHC and α-actin in cell lysate was determined by Western blot analysis. (*B*) Cachectic cancer cell–conditioned media induce up-regulation of UBR2 but not MuRF1. Myotubes were treated as described in *A* for 8 h. UBR2 and MuRF1 levels were analyzed by Western blotting. (*C*) Hsp70 and Hsp90 induce up-regulation of UBR2 but not MuRF1. Myotubes were treated with endotoxin-free recombinant Hsp70 and Hsp90 (100 ng/mL each) for 8 h. UBR2 and MuRF1 levels were analyzed by Western blotting. (*D*) UBR2 is critical for MHC loss induced by cachectic cancer cell–conditioned media. The *UBR2* gene in myotubes was knocked down by siRNA prior to treatment with conditioned medium of NL20 (NCM), LLC (LCM), or C26 (CCM) cells for 72 h. UBR2 and total MHC levels were analyzed by Western blotting. (*E*) UBR2 is critical for myotube atrophy induced by cancer cell–conditioned medium. Myotubes derived from *D* were subjected to immunostaining of total MHC and measurement of myotube diameters. (*F*) MuRF1 is not required for MHC loss induced by cancer cell–conditioned medium. The *MuRF1* gene in myotubes was knocked down by siRNA prior to NCM or LCM treatment for 72 h. MuRF1 and total MHC levels were analyzed by Western blotting. (*G*) MuRF1 is not required for myotube atrophy induced by cachectic cancer cell–conditioned media. Myotubes derived from *F* were subjected to immunostaining of MHC and myotube diameter was measured. (*H*) A dominant-negative mutant of UBR2 abrogates MHC loss induced by cachectic cancer cell–conditioned media. Empty vector or plasmid encoding DN-UBR2 was transfected into myotubes prior to treatment with LCM or CCM for 72 h. UBR2 and total MHC levels were analyzed by Western blotting. (*I*) A dominant-negative mutant of UBR2 abrogates MHC loss induced by recombinant Hsp70 and Hsp90. Myotubes transfected with empty vector or DN-UBR2 plasmid were treated with endotoxin-free Hsp70 and Hsp90 (100 ng/mL each) for 72 h. UBR2 and total MHC levels were analyzed by Western blotting. Data ($n = 3$) were analyzed using raw measurements by one-way ANOVA combined with Tukey's test. A difference from the control ($P < 0.05$) is indicated by *.

C2C12 myotubes stimulated by cancer cell–released catabolic factors, C2C12 myotubes overexpressing FLAG-tagged WT-UBR2, a UBR2 mutant with point mutations in its substrate recognition domain (SRDM-UBR2) (33), or the empty vector, were treated with LCM or control medium in the presence of proteasome inhibitor MG132. The cell lysates were subjected to pulldown assays using either beads that bind the FLAG tag or polyubiquitylated proteins (TUBE2). FLAG-tagged and total UBR2 content in cell lysates (input) as well as MHC and α-actin content in the pulled down pellet were analyzed by Western blotting. As shown in Fig. 4*A*, pulldown of FLAG-tagged WT-UBR2 resulted in coprecipitation of MHC with increasing molecular sizes consistent with polyubiquitylated MHC, which was further increased by LCM treatment. However, pulldown of FLAG-tagged SRDM-UBR2 failed to coprecipitate MHC. On the other hand, α-actin was not coprecipitated with either form of overexpressed UBR2. These data suggest that constitutive and LCM-stimulated polyubiquitylation of MHC requires an interaction between MHC and UBR2 through its substrate recognition domain. Concordantly, TUBE2 beads pulled down

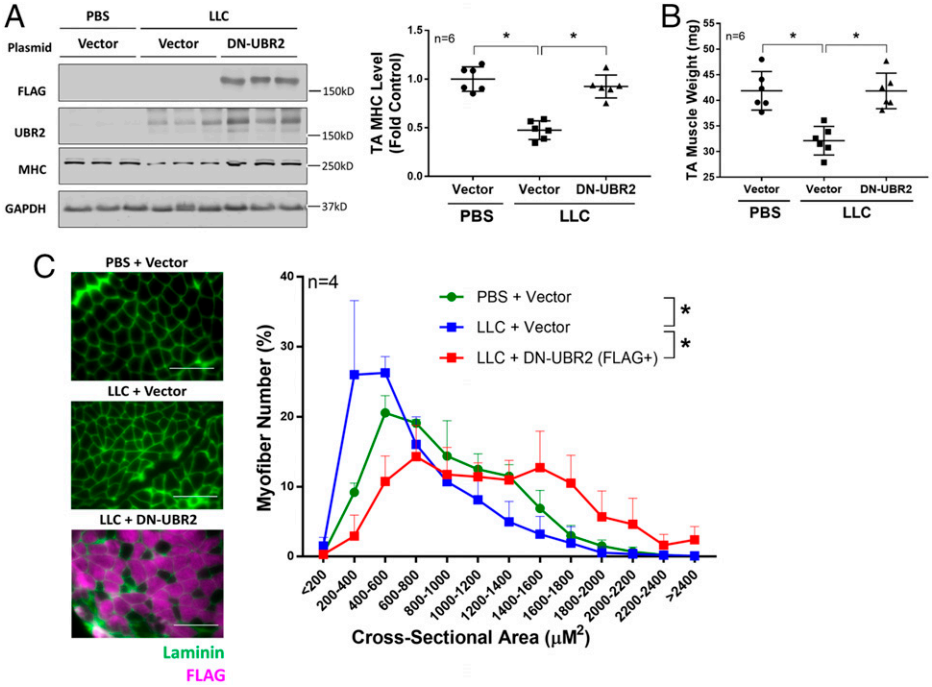

Fig. 2. UBR2 is critical for loss of MHC and muscle mass in TA of tumor-bearing mice. (*A*) UBR2 is critical for MHC loss in TA of LLC tumor–bearing mice. A plasmid encoding DN-UBR2 or empty vector was transfected into the contralateral TA of male mice bearing LLC tumor or PBS-injected control mice as indicated on day 7 and day 14 of tumor cell implant (n = 6). After cachexia has developed (day 21) TA content of FLAG-tagged DN-UBR2, UBR2 and total MHC were analyzed by Western blotting. (*B*) UBR2 is critical for loss of muscle weight in TA of LLC tumor–bearing mice. TA of the mice described in *A* was excised and weighed. (*C*) UBR2 is critical for loss of myofiber cross-sectional area in TA of LLC tumor–bearing mice with cachexia. Cross-sections of TA described in *A* were subjected to immunofluorescence staining of laminin and the FLAG tag on DN-UBR2 to trace myofibers that expressed DN-UBR2. (Scale bar, 50 μm.) Data were analyzed by one-way ANOVA combined with Tukey's test for *A* and *B*, and χ^2 test for *C*. A difference ($P < 0.05$) is indicated by *.

polyubiquitylated MHC from lysate of LCM-treated myotubes that were transfected with the empty vector and from lysate of myotubes that overexpressed WT-UBR2, which was further increased by LCM treatment. However, TUBE2 beads failed to pull down polyubiquitylated MHC from lysate of myotubes that overexpressed SRDM-UBR2. On the other hand, TUBE2 beads pulled down polyubiquitylated α-actin from LCM-treated myotubes independent of overexpressed WT-UBR2 or SRDM-UBR2. These data suggest that UBR2 mediates polyubiquitylation of MHC but not α-actin. In addition, the molecular sizes of detected MHC and α-actin indicated a marked difference in the length of the polyubiquitylation chain attached to the two proteins. Thrower et al. showed that a 6-fold increase in polyubiquitin chain length increases its affinity to proteasome by ∼600-fold, and that a four-unit polyubiquitin chain is the minimum signal required for proteasome binding (34). The molecular size of the polyubiquitylated α-actin indicates that it is at or below the minimum polyubiquitylation required for binding to proteasome. The marked difference in their polyubiquitylation chain length explains why MHC is highly degraded in response to cancer cell–conditioned medium in contrast to α-actin as seen in Fig. 1*A*. These data suggest that UBR2 interacts with MHC through its substrate-recognition domain to polyubiquitylate MHC in C2C12 myotubes.

To further verify that UBR2 mediates LCM-induced ubiquitylation of MHC in C2C12 myotubes through its catalytic domain, the DN-UBR2 mutant was overexpressed to replace SRDM-UBR2 in the pulldown experiment described above. As shown in Fig. 4*B*, pulldown of DN-UBR2 with FLAG-binding beads resulted in coprecipitation of MHC that was much less ubiquitylated in control or LCM-treated cell lysates, indicating that the catalytic domain of UBR2 was required for the basal and LCM-stimulated ubiquitylation of MHC. Further, the TUBE2 beads pulldown assay confirmed that in contrast to WT-UBR2, DN-UBR2 inhibited ubiquitylation of MHC. These data reveal that UBR2 ubiquitylates MHC through its catalytic domain in response to cancer cell–released catabolic factors.

To identify MHC subtypes ubiquitylated by UBR2, the above pulled down pallets were subjected to Western blot analysis with antibodies against MHC subtypes. We observed that MHC-IIb and -IIx, but not MHC-I and -IIa, were interacted with and ubiquitylated by UBR2 (Fig. 4*C*). These results suggest that MHC IIb and IIx are selectively ubiquitylated by UBR2.

UBR2 Selectively Targets MHC-IIb and -IIx for Degradation in Mouse Muscle. To verify the MHC subtypes targeted by UBR2 for degradation in vivo, WT-UBR2 was overexpressed in the gastrocnemius of cancer-free male mice containing both slow-twitching and fast-twitching myofibers. Using Western blot analysis of the homogenate of the entire gastrocnemius we observed that overexpression of WT-UBR2 resulted in ∼60% loss of total MHC, and ∼90% loss of MHC-IIb as well as ∼60% loss of MHC-IIx. However, levels of MHC-I and MHC-IIa were not altered (Fig. 5*A*). To verify the distribution of transgene expression in diverse types of myofibers, immunofluorescence staining of frozen sections of the transfected gastrocnemius was performed. Overexpressed WT-UBR2 with FLAG tag was detected in myofibers positive for MHC-I, -IIa, or -IIb; however, only MHC-IIb–positive myofibers lost cross-sectional area (*SI Appendix*, Fig. S5), confirming that the transgene was expressed in both fast and slow myofibers, however reducing the size of fast myofibers only.

To determine whether cancer induced UBR2 up-regulation and caused MHC loss in slow-twitching muscles, we examined soleus in control and KPC tumor–bearing male mice. As seen in TA, UBR2 was up-regulated by KPC in soleus. However, total MHC, MHC-I, and MHC-IIa levels were not altered (Fig. 5*B*). To further examine the selectivity of UBR2-mediated myofibrillar protein degradation, we measured the levels of troponin, tropomyosin, and tropomodulin in the TA of LLC and KPC tumor–bearing male mice that developed cachexia. None of these protein levels were altered (*SI Appendix*, Fig. S6), suggesting that these proteins are not targeted by UBR2 in cancer cachexia. These data indicate that despite cancer up-regulating UBR2 in both fast- and slow-twitching muscles, UBR2 selectively targets MHC IIb and IIx for degradation.

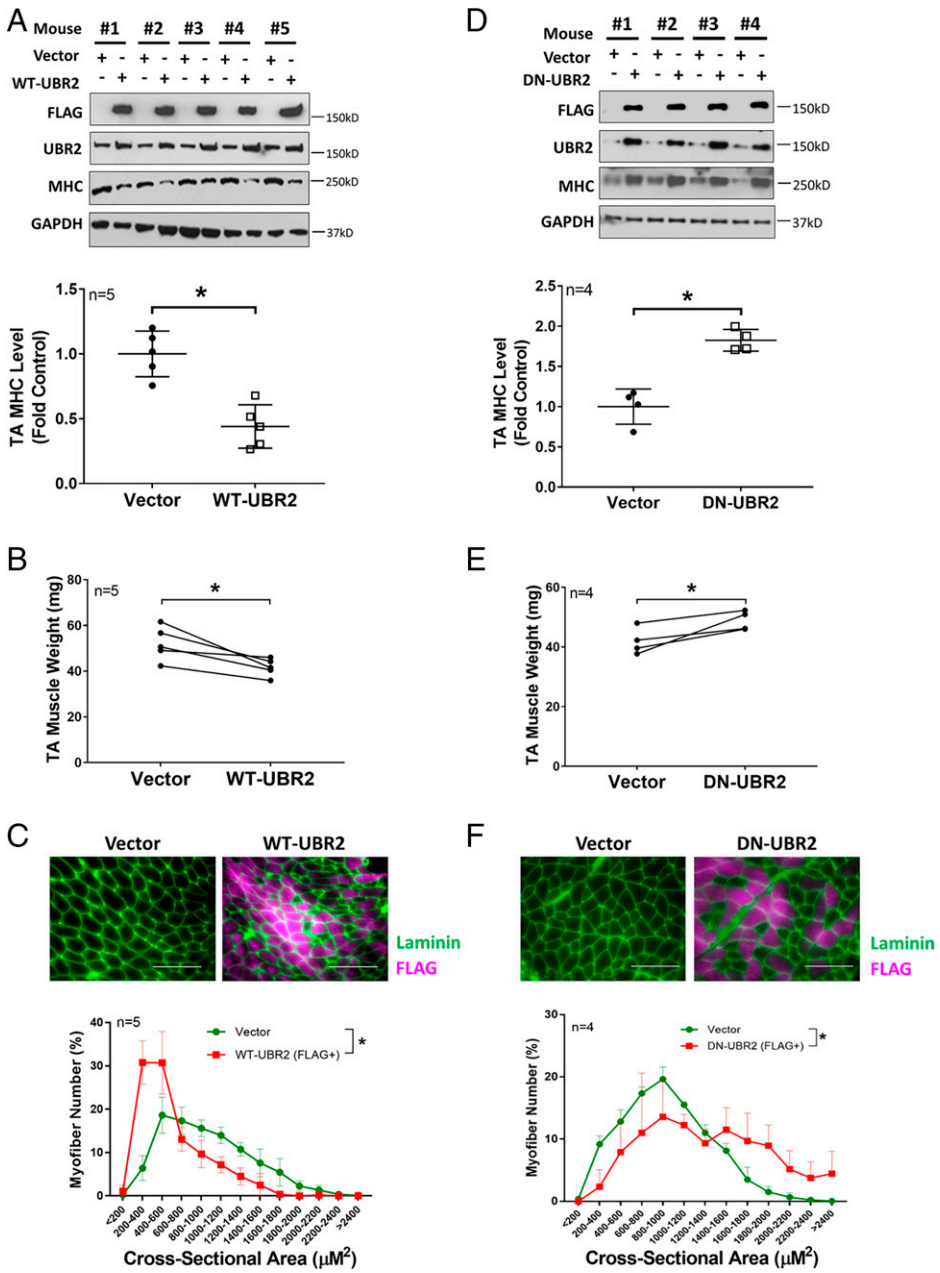

Fig. 3. UBR2 regulates MHC and muscle mass in TA of tumor-free mice. (*A*–*C*) Overexpression of WT-UBR2 in TA of cancer-free mice reduces MHC content, muscle weight, and the myofiber cross-sectional area. Contralateral TA of cancer-free male mice was transfected with plasmid encoding either WT-UBR2 or empty vector on day 0 and 7 ($n = 5$). On day 14 UBR2 and total MHC content were analyzed by Western blotting (*A*), muscle mass was evaluated by muscle weight (*B*) and FLAG-positive myofiber cross-sectional area (*C*). (*D*–*F*) Overexpression of DN-UBR2 increases MHC content, muscle weight, and myofiber cross-sectional area in normal TA. Contralateral TA of cancer-free male mice was transfected with plasmid encoding either DN-UBR2 or empty vector as described above ($n = 4$); UBR2 and total MHC content were analyzed by Western blotting (*D*); and muscle mass was evaluated by muscle weight (*E*) and FLAG-positive myofiber cross-sectional area (*F*). (Scale bar, 50 μm.) Data were analyzed by paired Student's *t* test for *A*, *B*, *D*, and *E*, and by χ^2 test for *C* and *F*. A difference ($P < 0.05$) is indicated by *.

Skeletal Muscle-Specific Knockout of UBR2 Protects Tumor-Bearing Mice from Losing Fast-Twitching Muscle Mass and Function. To assess whether UBR2 is critical for cancer-induced muscle wasting, we generated a UBR2-floxed mouse line ($UBR2^{fl/fl}$) and crossed it to the MCK-Cre mouse line to specifically knock out UBR2 in fast and slow-twitching skeletal muscles (*SI Appendix*, Fig. S7 *A*–*C*). Phenotypic studies revealed that the resulting mouse line UBR2-mKO did not have changes in MHC isoform distribution (*SI Appendix*, Fig. S7*D*), body and muscle weight, myofiber cross-sectional area, and muscle contractility (Fig. 6). In addition, UBR2 deletion did not alter the basal expression of *MAFbx* and *MuRF1* mRNA (*SI Appendix*, Fig. S8*A*). On the other hand, the basal level of another UBR family member UBR1 (also known as E3α-I) (35) increased in the TA of UBR2-mKO mice (*SI Appendix*, Fig. S8*B*). In comparison, UBR1 level in mouse TA overexpressing DN-UBR2 acutely described in Fig. 3 was not significantly increased (*SI Appendix*, Fig. S8*C*), suggesting that the UBR1 level may increase over a longer period as compensation for the chronic loss of UBR2. Utilizing the KPC orthotopic xenograft model (31) we observed that male $UBR2^{fl/fl}$ mice developed severe cachexia on day 21 after tumor cell implant as indicated by a 17% loss of body weight, which was attenuated in male UBR2-mKO mice (Fig. 6*A*). Given that the KPC tumor also induces fat tissue loss (31) we examined the effect of UBR2 deletion on the weight of epididymal and subcutaneous fat pads. The tumor caused a nearly

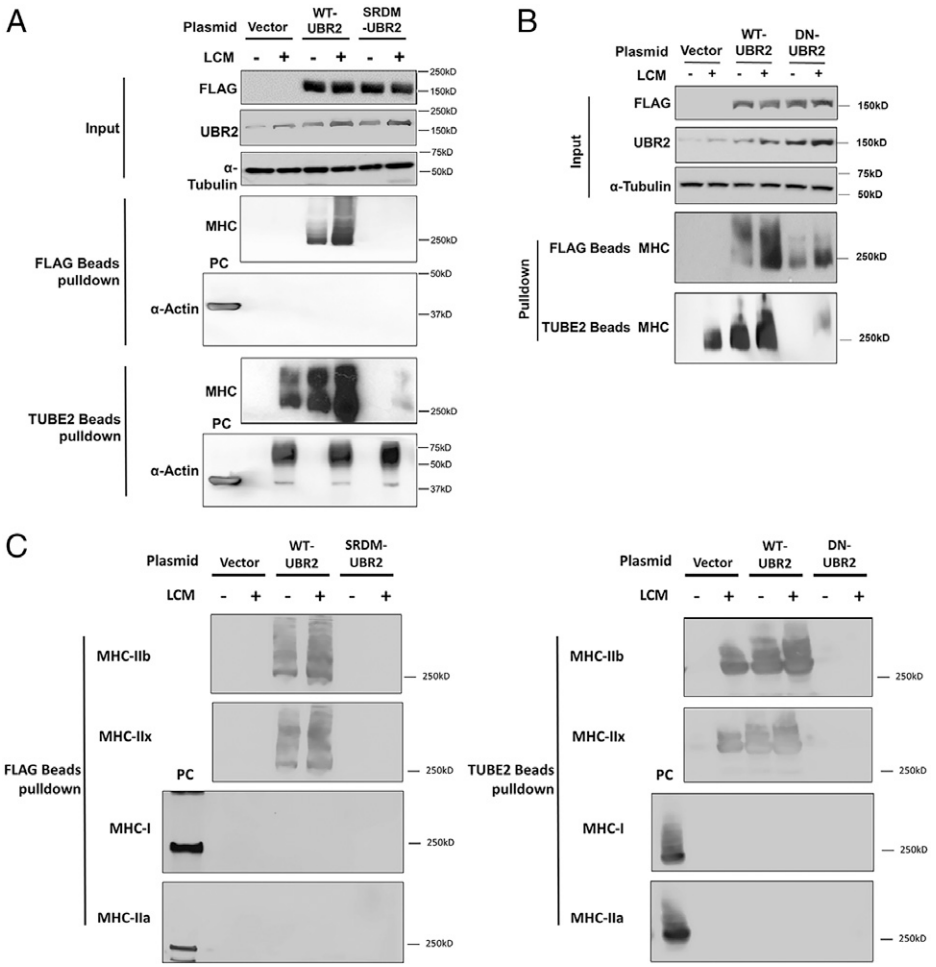

Fig. 4. UBR2 selectively ubiquitylates MHC-IIb and MHC-IIx in C2C12 myotubes. (*A*) UBR2 selectively ubiquitylates MHC through an interaction with its substrate recognition domain. C2C12 myotubes transfected with empty vector, FLAG-tagged WT-UBR2, or SRDM-UBR2 (UBR2 with point mutations in its substrate recognition domain) were treated with LCM for 8 h in the presence of proteasome inhibitor MG132 (10 μM). Cell lysate was subjected to pulldown assay using either FLAG-binding beads or TUBE2 beads that bind polyubiquitinated proteins. UBR2 content in cell lysate (input) and total MHC or α-actin content in pulled down pellet were analyzed by Western blotting. For α-actin detection, lysate of control C2C12 myotubes was used as positive control (PC). (*B*) UBR2 ubiquitylates MHC through its catalytic domain. C2C12 myotubes transfected with empty vector, FLAG-tagged WT-UBR2, or DN-UBR2 were subjected to LCM treatment and pulldown assay as described in *A*. (*C*) UBR2 interacts with and ubiquitylates MHC-IIb and -IIx but not MHC-I and -IIa. The above pulled down pellets were further analyzed by Western blotting with antibodies specific for MHC subtypes. For MHC-I and -IIa detection lysate of C2C12 myotubes was used as PC.

total loss of both fat tissues in UBR2$^{fl/fl}$ and UBR2-mKO mice similarly in both sexes (*SI Appendix*, Fig. S9). In addition, tumor volume was not altered by UBR2 deficiency (Fig. 6*B*). On the other hand, muscle-specific deletion of UBR2 prevented the ≥30% weight loss in muscles containing fast-twitching myofibers, including TA, extensor digitorum longus (EDL), and gastrocnemius, while weight of slow-twitching muscle soleus was not affected by either tumor or UBR2 knockout (Fig. 6*C*). The latter was consistent with the preservation of MHC content observed in soleus of KPC tumor–bearing mice (Fig. 5*B*). In examining catabolic markers we found that while the KPC tumor caused up-regulation of UBR2 and ∼60% loss of total MHC in the TA of UBR2$^{fl/fl}$ mice, UBR2-mKO mice were resistant to MHC loss. Further analysis of MHC subtypes revealed that the KPC tumor caused a selective loss of MHC-IIb and MHC-IIx, but not MHC-IIa, in a UBR2-dependent manner. Consistent with the in vitro data of Fig. 1*A*, the α-actin level in TA was not altered by the tumor (Fig. 6*D*). On the other hand, the KPC tumor induced up-regulation of *MAFbx* and *MuRF1* mRNA in the TA of UBR2$^{fl/fl}$ mice, which was further increased in UBR2-mKO mice (*SI Appendix*, Fig. S8*A*). KPC tumors also up-regulated UBR1 in the TA of UBR2$^{fl/fl}$ and UBR2-mKO mice (*SI Appendix*, Fig. S8*B*). Moreover, KPC tumors induced an increase of LC3-II, a marker of autophagy, in UBR2$^{fl/fl}$ and UBR2-mKO mice similarly (Fig. 6*D*). Consequently, UBR2-mKO mice were spared from tumor-induced loss of myofiber cross-sectional area (Fig. 6*E*) and minimum Feret diameter (*SI Appendix*, Fig. S3*D*) in TA. Remarkably, while the KPC tumor caused an ∼50% loss of the contractile force generated ex vivo by EDL of UBR2$^{fl/fl}$ mice, EDL of UBR2-mKO mice retained nearly the total force generation capacity (Fig. 6*F*, unnormalized force generation is shown in *SI Appendix*, Fig. S10), indicating that UBR2-mediated loss of MHC-IIb and -IIx is responsible for the contractile dysfunction in cancer cachexia.

In female mice, the basal expression of UBR2 in TA is not different from male mice (*SI Appendix*, Fig. S11*A*). In female UBR2$^{fl/fl}$ mice KPC tumors caused muscle wasting 4 d later than their male counterparts, which was similarly abrogated in female UBR2-mKO mice without altering tumor growth (*SI Appendix*, Fig. S11). These data indicate a similar role of UBR2 in female mice. On the other hand, KPC-induced body weight loss was not protected in female UBR2-mKO mice (*SI Appendix*, Fig. S11*B*), possibly due to the fact that female mice have a smaller muscle mass (*SI Appendix*, Fig. S11 *D* and *E*) and a larger fat mass (*SI Appendix*, Fig. S9) as percentages of body weight (*SI Appendix*, Fig. S11*B*) in comparison to male mice (Fig. 6 *A* and

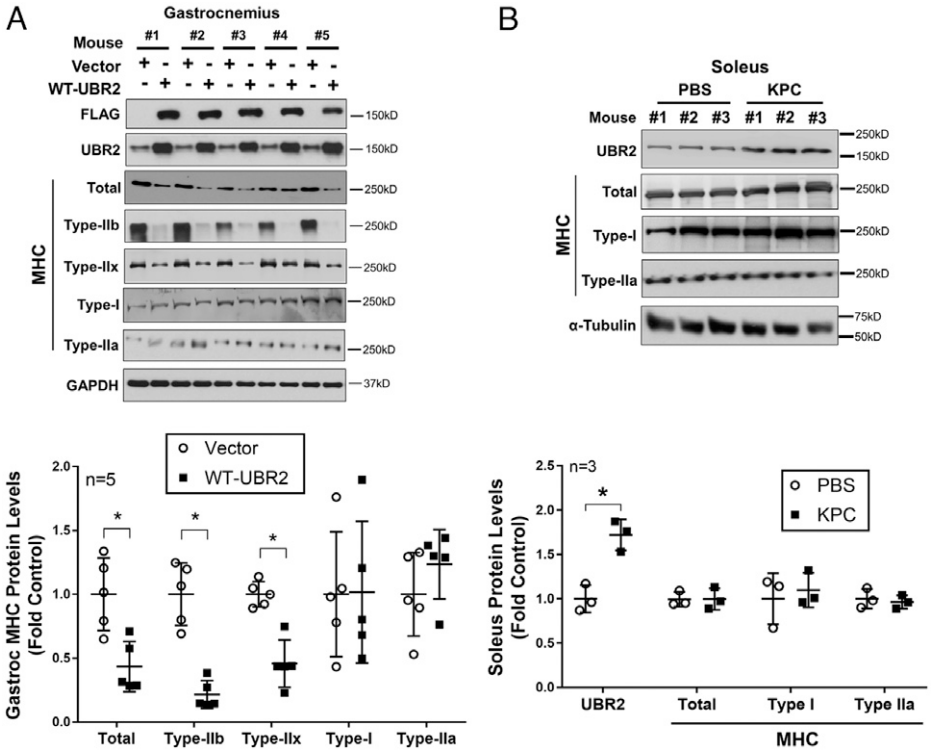

Fig. 5. UBR2 selectively targets MHC-IIb and -IIx for degradation in mouse muscle. (*A*) Overexpressed WT-UBR2 in gastrocnemius causes loss of MHC-IIb and -IIx but not MHC-I and -IIa. Gastrocnemius of male cancer-free mice ($n = 5$) was transfected with empty vector or FLAG-tagged WT-UBR2 on days 0 and 7. On day 14, content of UBR2 and MHC (total and isoforms) were analyzed by Western blotting. Data were analyzed by paired Student's *t* test. (*B*) KPC tumor does not cause loss of oxidative MHCs (I and IIa) in soleus despite up-regulation of UBR2. KPC cells were orthotopically implanted into male mice ($n = 3$). On day 21 content of UBR2 and MHC (total and isoforms) in soleus was analyzed by Western blotting. Data were analyzed by Student's *t* test. * indicates a difference ($P < 0.05$).

C) (36), such that the improvement in muscle mass loss was not sufficient to counter the effect of the dramatic loss of fat mass (*SI Appendix*, Fig. S9) on body weight.

To further verify the necessary and sufficient role of UBR2 in mediating MHC loss in cancer cachexia, WT-UBR2 was overexpressed in the TA of male UBR2-mKO mice bearing the KPC tumor, which restored MHC loss in the TA of UBR2-mKO mice (*SI Appendix*, Fig. S12). These data identify UBR2 as a key mediator of cancer-induced muscle wasting due to its essential role in the loss of MHC-IIb/IIx and contractile force of fast-twitching muscles.

MHC-IIx Is Selectively Lost in Skeletal Muscle of Cancer Patients in Correlation with UBR2 Up-Regulation. To determine whether cachectic cancer patients suffer from UBR2-mediated selective loss of specific MHC subtypes as observed in tumor-bearing mice, we examined the RA muscle collected from cancer patients in a previous study (22). In that study, male patients with diverse types of cancer in the GI or GU tract who were either weight loss (CWL) or weight stable (CWS) were compared with weight stable noncancer subjects (NCC, $n = 20$/group). We found that RA of CWS and CWL possessed higher levels of UBR2 and lower levels of total MHC in comparison to the NCC group. Importantly, UBR2 levels were progressively higher in CWL than CWS. However, total MHC was not different between CWL and CWS. On the other hand, levels of α-actin remained same in all three groups (22). Given the findings on the role of UBR2 in the current study, we further investigated whether UBR2 up-regulation was associated with a selective loss of fast MHC in these cancer patients by analyzing levels of MHC subtypes in RA. Human skeletal muscle contains three MHC subtypes (I, IIa, and IIx) (37). As shown in Fig. 7*A*, we found that levels of MHC-I and MHC-IIa were not different in all three groups. However, levels of MHC-IIx were lower in CWS and further lower in CWL, indicating that MHC-IIx was selectively lost in cancer patients in association with weight loss as seen in tumor-bearing mice. To examine whether loss of MHC-IIx correlated with UBR2 up-regulation, levels of each of the MHC subtypes examined in all 60 samples were plotted against previously determined UBR2 levels in the same samples (22). A significant inverse correlation was detected between the levels of UBR2 and MHC-IIx, but not between UBR2 and MHC-I or MHC-IIa (Fig. 7 *B*–*D*). In addition, levels of troponin, tropomyosin, and tropomodulin were the same in the three groups (*SI Appendix*, Fig. S13) as seen in murine cancer models (*SI Appendix*, Fig. S6). These data confirm in cancer patients that the increase of UBR2 correlates with the selective loss of MHC-IIx.

Discussion

The current study identifies a pathological as well as a physiological role of UBR2 in targeting MHC-IIb and MHC-IIx for degradation that is essential for cancer-induced muscle wasting. Utilizing cell culture and murine models of cancer cachexia, we show that diverse types of cachexia-prone cancer induce loss of MHC selectively in fast-twitching myofibers, particularly MHC-IIb and -IIx, through the E3 ubiquitin ligase UBR2, resulting in loss of myofiber mass and contractile force in fast-twitching muscle. Further, our data verify in human skeletal muscle that cachexia-prone cancers are associated with a preferential loss of MHC-IIx in correlation with an increase in UBR2 level. Thus, UBR2 appears to be a key mediator of cancer-induced muscle wasting.

In contrast to MuRF1, we found that UBR2 was consistently up-regulated in C2C12 myotubes by diverse types of cachexia-prone cancer cell–conditioned medium. Importantly, cancer

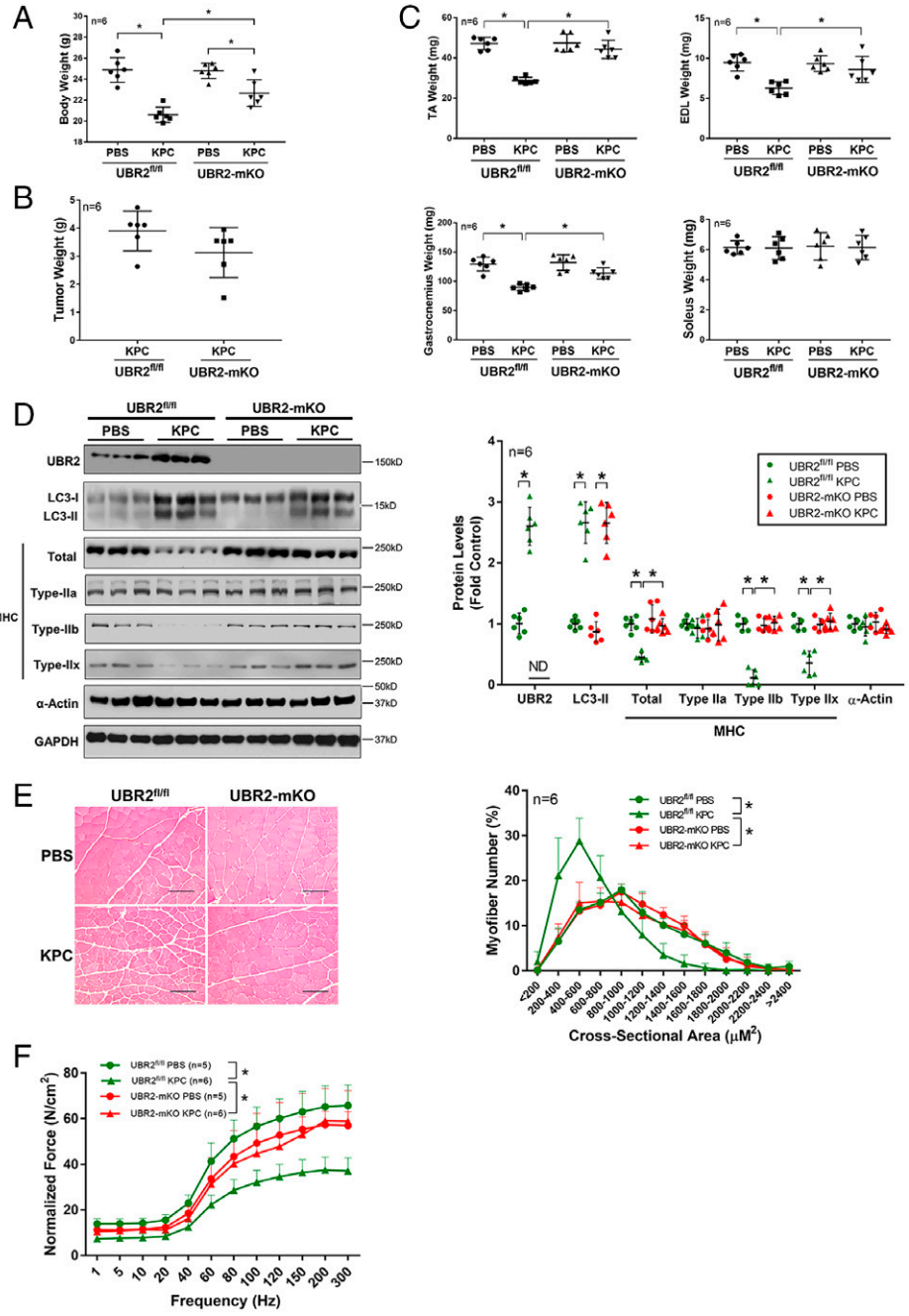

Fig. 6. KPC tumor–induced muscle wasting is abrogated in UBR2 muscle–specific knockout mice. Male UBR2-floxed ($UBR2^{fl/fl}$) or UBR2 muscle–specific knockout mice (UBR2-mKO) were orthotopically implanted with KPC cells or PBS as control ($n = 6$). In 21 d, mice were killed and analyzed for muscle wasting. (*A*) UBR2-mKO mice have similar body weight as $UBR2^{fl/fl}$ mice and are resistant to KPC tumor–induced body weight loss (excluding tumor weight). (*B*) Tumor growth is not altered in UBR2-mKO mice. (*C*) UBR2-mKO mice have similar muscle weight as $UBR2^{fl/fl}$ mice and are resistant to KPC tumor–caused weight loss of muscles containing fast-twitching myofibers (TA, EDL, and gastrocnemius). (*D*) UBR2-mKO mice have similar levels of MHC isoforms and α-actin as $UBR2^{fl/fl}$ mice and are spared from KPC tumor–induced loss of total and MHC-IIb and -IIx in TA. (*E*) UBR2-mKO mice have a similar myofiber cross-sectional area as $UBR2^{fl/fl}$ mice and are spared from KPC tumor–induced loss of myofiber cross-sectional area in TA. (Scale bar, 50 μm.) (*F*) UBR2-mKO mice have similar muscle contractile force as $UBR2^{fl/fl}$ mice and are protected from KPC tumor–induced loss of muscle contractile force. Data were analyzed by two-way ANOVA combined with Tukey's test (*A*–*D* and *F*) or χ^2 test (*E*). A difference ($P < 0.05$) is indicated by *.

cell–conditioned media-induced MHC loss required UBR2 but not MuRF1 (Fig. 1). On the other hand, the *MuRF1* mRNA was up-regulated in the TA of KPC tumor–bearing mice (*SI Appendix*, Fig. S8*A*), suggesting its up-regulation in vivo is mediated indirectly by a body response to tumors, rather than a direct response to tumor cell–released catabolic factors such as Hsp70 and Hsp90 (Fig. 1*C*). Nevertheless, despite the up-regulation of *MuRF1*, *MAFbx*, and UBR1 by KPC in UBR2-mKO mice, loss of MHC-IIb/IIx and fast-twitching muscle mass/function were largely prevented. These data support a key role of UBR2 in mediating proteasomal degradation of MHC in fast-twitching muscle in response to a tumor burden.

Our data also demonstrate that UBR2 level/activity inversely correlates with muscle mass and MHC levels in fast-twitching muscles of adult cancer-free mice that were subjected to acute changes in UBR2 content/activity by genetic manipulations, suggesting that UBR2 maintains homeostasis of fast-twitching muscle mass under physiological conditions. On the other hand, UBR2-mKO mice did not display significant phenotypical alterations in fast-twitching muscles due possibly to compensatory

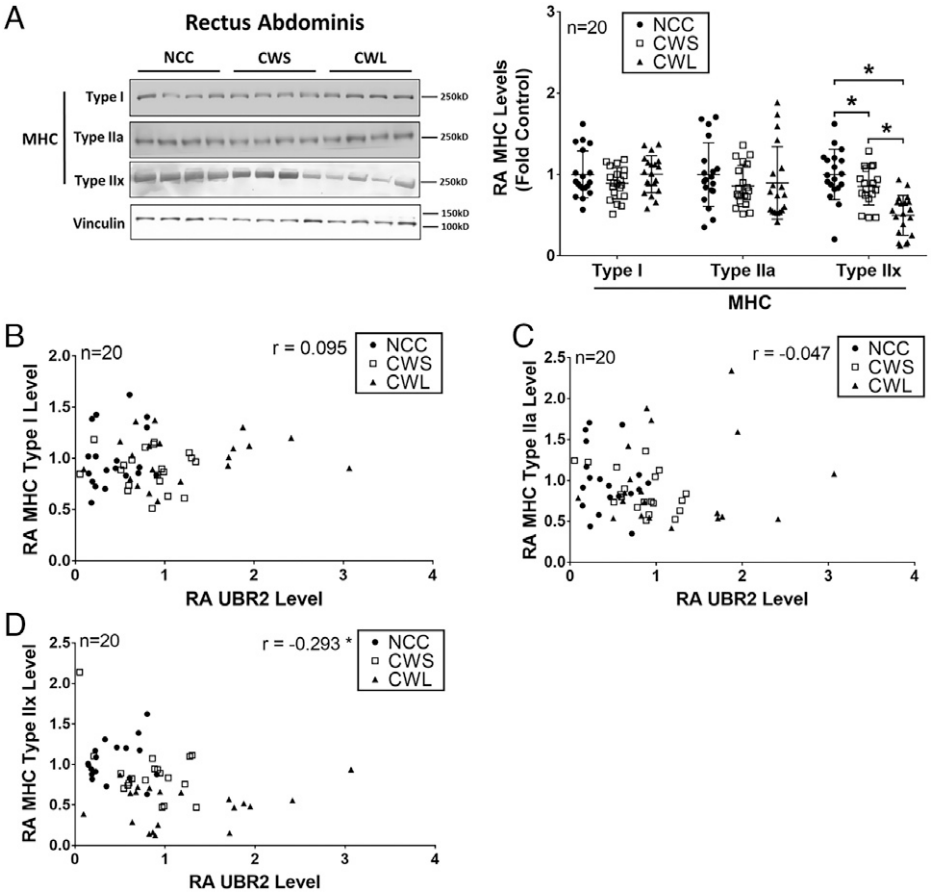

Fig. 7. Myosin heavy chain IIx is selectively lost in cancer patient skeletal muscle in correlation with UBR2 up-regulation. (*A*) Levels of MHC isoforms (I, IIa, and IIx) in rectus abdominis (RA) collected from noncancer control (NCC), cancer with weight stable (CWS), and cancer with weight loss (CWL) groups (n = 20/group) were analyzed by Western blotting. Representative blots are shown. *P < 0.05, determined by one-way ANOVA combined with Tukey's test. (*B–D*) Levels of MHC I, IIa, and IIx detected in all patient RA samples were plotted against previously detected levels of UBR2 in the same samples (22). Correlation between the levels of each of the MHC subtypes and UBR2 levels in the 60 human subjects was determined by Pearson's correlation coefficient test. *P < 0.05.

adjustments of other components of the UPP such as increased expression of UBR1 over the longer term (*SI Appendix*, Fig. S8 *B* and *C*). As one of the catabolic genes up-regulated by the p38β MAPK–p300–C/EBPβ signaling pathway that is critical for muscle wasting in cancer (21, 24–26, 38), UBR2 knockout is expected to have an impact on cancer-induced muscle wasting. Nevertheless, it was surprising that UBR2 deletion abolished the loss of fast-twitching muscle mass and function almost completely in KPC tumor–bearing mice, considering that levels of other components of the UPP, such as *MAFbx*, *MuRF1*, and UBR1, as well as the ALP, such as LC3-II, remained elevated or further increased. These observations suggest that UBR2-mediated loss of MHC-IIb and MHC-IIx are responsible for the bulk of loss of fast-twitching muscle mass and function in cancer cachexia. A previous study on single myofibers revealed that type IIx fiber generates twice as much power as type IIa fiber, while the latter is four times more powerful than type I fiber. Therefore, type IIx fiber is considered superfast (39). The preferential loss of MHC-IIx explains the devastating effect of cancer cachexia on muscle function. These data also explain why cancer-induced muscle mass loss is different from denervation or disuse-induced muscle mass loss. The latter two preferentially cause loss of MHC-I/IIa and slow-twitching muscle mass through MuRF1 up-regulation mediated by the AKT-FOXO signaling pathway (40–42).

We observed that other myofibrillar proteins including α-actin, troponin, tropomyosin, and tropomodulin are not lost in murine cancer models, which is consistent with a previous report (43). In addition, α-actin (22) as well as troponin, tropomyosin, and tropomodulin are not lost in RA of cancer patients who lost MHC-IIx (*SI Appendix*, Fig. S13). Our in vitro analyses (Fig. 4) pinpointed the specific interaction of UBR2 with MHC-IIb and -IIx in C2C12 myotubes through its substrate recognition domain, enabling it to polyubiquitylate these MHC subtypes through its catalytic domain. In contrast, α-actin is insufficiently polyubiquitylated in response to cancer cell–released factors in a UBR2-independent manner, which explains the resistance of α-actin to cancer-induced myofibrillar protein degradation observed in vitro (Fig. 1*A*) and in vivo (Fig. 6*D*). Further, UBR2 was similarly up-regulated in soleus of tumor-bearing mice without causing loss of MHC-I and MHC-IIa (Fig. 5*B*), indicating that the signaling mechanism regulating UBR2 is present in both slow and fast-twitching muscles, but UBR2 selectively targets MHC-IIb and MHC-IIx to cause loss of fast-twitching muscle mass.

Although autophagy activation in cachectic muscle has been consistently observed in rodent and human cancer cachexia (44), its precise role in muscle wasting remains undefined. The data that despite an increase in autophagy marker LC3-II, UBR2 deletion alone was sufficient to abrogate the loss of fast-twitching muscle fiber mass and function in tumor-bearing mice (Fig. 6) support a dominant role of UPP in muscle wasting associated with cancer cachexia. On the other hand, autophagy may have a role in the organelle dysfunctions associated with cancer-induced

muscle wasting through impairing mitochondrial (45) and endoplasmic reticulum functions (46).

The N-end rule pathway targets proteins that possess basic or large hydrophobic amino acids at the N terminus (47). Because muscle proteins do not have such features in the normal state, it is thought that the N-end rule pathway works in part through destabilized N-terminal residues that are generated in soluble proteins (48). One possibility is that MHC-IIb and MHC-IIx are cleaved near the N termini by endopeptidases to generate an N degron that interacts with UBR2. Whether this is the case is yet to be determined.

In a previous cancer patient study (22), we observed a progressive increase of UBR2 in CWL and CWS over NCC, suggesting its association with muscle wasting. However, MuRF1 levels (mRNA and protein) in CWL and CWS were the same as in NCC. The lack of MuRF1 up-regulation in cancer patients who developed muscle wasting was consistent with previous reports (49–52), suggesting that UBR2 plays an important role in cancer-induced muscle wasting in humans. On the other hand, our previous study found that loss of total MHC in cancer patients was similar in CWS and CWL (22). In the present study, we further observed that cancer patients suffered a progressive loss in MHC-IIx that was greater in CWL than in CWS, while MHC-I and MHC-IIa remained unchanged, revealing an inverse correlation between UBR2 and MHC-IIx levels. These data support a key role of UBR2 in targeting MHC-IIx for degradation in cancer patients. It is noteworthy that the patients we studied were in relatively earlier stages of cancer with less advanced cachexia (22). Similarly, a previous clinical study (53) detected preferential loss in the cross-sectional area of fast myofibers in cancer patients with less advanced cachexia (classes I and II). However, in patients with more advanced cachexia (classes III and IV) loss in the cross-sectional area of both fast and slow myofibers was detected, suggesting that with disease progressing MHC I and MHC IIa can eventually be affected. Patients with more advanced cachexia usually experience longer-term deterioration of physical conditions, including fatigue, inactivity, and malnutrition, which may contribute to the muscle wasting in addition to cancer per se through the AKT-FOXO signaling pathway to up-regulate MuRF1 (40–42) and cause loss of MHC I and IIa.

Clinical trials of cancer cachexia interventions employing various strategies so far have not yielded satisfactory results (54, 55). Even though in some cases, including anamorelin, muscle mass was restored due to improved nutritional status, muscle function was not (56). In this regard, our data that deleting UBR2 protected fast muscle mass and function in tumor-bearing mice suggests that an effective intervention of cancer cachexia should have the capacity to protect MHC-IIb/IIx from UBR2-mediated degradation. Thus, strategies for inhibiting UBR2 or its up-regulation by p38β MAPK and p300 (25, 38) could be developed for intervening cancer cachexia.

Materials and Methods

Detailed information on cell lines, antibodies, analytical kits, and special reagents are listed in *SI Appendix*, Table S1.

Cell Culture. Murine C2C12 myoblasts were cultured in growth medium (Dulbecco's Modified Eagle Medium [DMEM] supplemented with 10% fetal bovine serum [FBS]) at 37 °C under 5% CO_2. At 85 to 90% confluence, myoblast differentiation was induced by incubation in differentiation medium (DMEM supplemented with 4% heat-inactivated horse serum) for 96 h to form myotubes. Tumor cell lines, including LLC, C26 (National Cancer Institute), H1299, BxPC-3 (American Type Culture Collection [ATCC]), and KPC (a gift from Elizabeth Jaffee, Johns Hopkins University, Baltimore, MD) (30) were cultured in RPMI1640 supplemented with 10% FBS. The nontumorigenic NL20 cells (ATCC) were cultured in Ham's F-12 medium supplemented with 1.5 g/L sodium bicarbonate, 2.7 g/L glucose, 2.0 mM L-glutamine, 0.1 mM nonessential amino acids, 0.005 mg/mL insulin, 10 ng/mL epidermal growth factor, 0.001 mg/mL transferrin, 500 ng/mL hydrocortisone, and 4% FBS following the supplier's instructions. All cells were cultured in 10-cm^2 culture plates. Conditioned medium from 48-h cultures of tumor cells or NL20 cells was collected and centrifuged (1,000 × *g*, 5 min). The supernatant was used to treat C2C12 myotubes (25% total volume) for indicated time periods and replaced every 24 h. In some experiments, myotubes were treated with endotoxin-free recombinant Hsp70 and Hsp90 (19) for indicated periods. All cell culture–based experiments were replicated three times independently.

Animal Use. All studies were conducted according to the National Institutes of Health Guide for the Care and Use of Laboratory Animals. Experimental protocols were approved in advance by the institutional Animal Welfare Committee at the University of Texas Health Science Center at Houston. Experimental mice were group housed, kept on a 12 h:12 h light/dark cycle with access to standard rodent chow and water ad libitum. The LLC cell subcutaneous xenograft was generated as previously described (19) in 8-wk-old C57BL/6J mice (The Jackson Laboratory). The KPC cell orthotopic xenograft was conducted following a published protocol (31). Briefly, 2×10^5 KPC cells (resuspended in 20 μL Phosphate buffered saline [PBS] containing 50% Matrigel or equal volume of PBS containing 50% Matrigel as control) were injected into the tail of the pancreas of 8-wk-old C57BL/6J mice under anesthesia. The openings in muscle and skin were sutured or sealed by wound clips, respectively. Development of cachexia was monitored by body weight and forelimb grip strength. Mice were killed and analyzed after cachexia had been established on day 21 post cancer cell implant for males, or day 24 for females.

Generation of Mice with Muscle-Specific Knockout of UBR2. $Ubr2^{tm1a(KOMP)Mbp}$ targeted embryonic stem (ES) cells were obtained from the KOMP Repository, University of California, Davis. The ES cells were microinjected into mouse embryos to generate $Ubr2^{tm1a(KOMP)Mbp}$ mice by the Transgenic and Stem Cells Service Center of University of Texas Health Science Center at Houston. $Ubr2^{tm1a(KOMP)Mbp}$ mice were crossed to Flpe (B6.129S4-Gt(ROSA)26-$Sor^{tm1(FLP1)Dym}$/RainJ, Jackson 009086) mice to remove the selection/reporter cassette. The resulting UBR2 floxed ($UBR2^{fl/fl}$) mice were then crossed to MCK-Cre mice (B6.FVB(129S4)-Tg(Ckmm-cre)5Khn/J, Jackson 006475) to generate mice with homozygous muscle-specific knockout of UBR2 (UBR2-mKO). Genomic DNA samples were prepared from tail and ear clippings using the HotSHOT method (57). Genotyping for $UBR2^{fl/fl}$ and wild-type alleles used the following primer pairs: GAGATGGCGCAACGCAATTAATG/CCAATCAACTTAGGAAAACCTTCACC, and CGACTAGCCTGTAGGTCTGTCTTGC/CTTTCTTAATGAGATTGCAGAGGTTCC, respectively. Genotyping for the Cre allele was performed with primers GTGAAACAG CATTGCTGTCACTT and TAAGTCTGAACCCGGTCTGC. The reactions were performed separately, using Thermo DreamTaq Green DNA polymerase (Thermo Fisher Scientific) with annealing temperature of 55 °C for both reactions and 35 amplification cycles. The PCR products were separated with electrophoresis using 2% agarose-TAE gel electrophoresis (*SI Appendix*, Fig. S5*A*). UBR2 protein levels in various organs (*SI Appendix*, Fig. S5*B*) and muscles (*SI Appendix*, Fig. S5*C*) were analyzed by Western blotting.

Patient Samples. Deidentified patient RA samples were obtained previously as described by Zhang et al. (22).

Plasmids. We generated plasmids encoding FLAG-tagged wild-type UBR2 (WT-UBR2), dominant negative mutant of UBR2 in which C1168 and H1170 residues in the RING finger (17) were replaced by alanine (DN-UBR2), and substrate recognition domain mutant of UBR2 in which D118 and N233 residues (33) were replaced by alanine (SRDM-UBR2). The endotoxin-free plasmid was prepared by PureYield Plasmid Midi kit (Promega Corporation) following manufacturer's instructions.

In Vitro Transfection. Plasmids or siRNAs were transfected into C2C12 myoblasts using the JetPrime transfection reagent (Polyplus-Transfection) following manufacturer's instructions when cells reached ∼60% confluence. Myoblasts were transferred to differentiation medium after a 24-h incubation of culture medium containing transfection mixture. The myoblasts were differentiated for 96 h before indicated treatments.

Magnetic Beads Pulldown Assay. The C2C12 myotubes transfected with control vector or plasmids overexpressing FLAG-tagged UBR2 proteins were treated with NL20 or LLC conditional medium for 8 h in the presence of proteasome inhibitor MG132 (10 μM). Samples were then divided into two portions for pulldown assays. Overexpressed UBR2 proteins in cell lysate were pulled down with FLAG-M2 magnetic beads (Sigma-Aldrich), and polyubiquitylated proteins were pulled down by TUBE2 magnetic beads (LifeSensors Inc.) following manufacturer's instructions. Pulldown samples were analyzed by Western blotting. Experiments were independently repeated for validation of the results.

In Vivo Transfection. The TA or gastrocnemius muscles of 8- to 9-wk-old male C57BL6/J mice were transfected with plasmid encoding FLAG-tagged WT-UBR2 or DN-UBR2 in one leg and the empty vector in the contralateral leg using a protocol modified from a previous report (58). Briefly, mice under anesthesia were injected with 15 units of hyaluronidase type IV-S in the muscles to be transfected, followed by plasmid injection (50 μg) in 2 h at multiple locations. The muscles were then stimulated by 10 electrical pulses (100 V/cm lasting 1 s with intervals of 1 s) generated by BTX T820 Electro Square Porator (Harvard Apparatus). The procedure was repeated in 7 d to increase transfection efficiency. Mice were killed 7 d after the second transfection for examination (21 d post tumor cell implantation).

Histology Analysis. To measure myotube diameters, C2C12 myotubes were fixed and permeabilized by ice-cold acetone, blocked by 5% bovine serum albumin (BSA) in PBS and stained with anti-MHC antibody (MF-20) followed by FITC-conjugated secondary antibody. To measure muscle fiber size or fiber type composition, the distal part of TA or gastrocnemius muscles were fixed by 4% paraformaldehyde PBS solution or snap frozen by liquid nitrogen precooled 2-methylbutane. The paraffin embedded cross-sections of 5-μm thickness were subjected to either hematoxylin and eosin (H&E) staining (conducted by the Pathology Core Lab at Baylor College of Medicine, Houston, TX) or immunofluorescence staining using antibodies against FLAG peptide (labeled by Alexa 647 conjugated secondary antibody) and laminin (labeled by Alexa 488 conjugated secondary antibody) antibody. Cryonic cross-sections (5-μm thickness) were fixed by methanol and costained by antibodies against FLAG (labeled by Alexa 594 conjugated secondary antibody), laminin and certain MHC subtype (labeled by Alexa 488 conjugated secondary antibody). To determine muscle fiber type composition, fixed cryonic cross-sections were step wisely stained by MHC I, MHC IIa, and MHC IIb antibodies, which were labeled by Alexa 488, Alexa 405, and Alexa 594 conjugated secondary antibodies, respectively. Fibers that could not be stained by any of these antibodies were considered as type IIx fibers. In all immunofluorescence experiments, the M.O.M. kit (Vector Laboratories) was used to minimize the background caused by anti-mouse secondary antibodies. Stained myotubes and muscle sections were examined and photographed using a Zeiss Axioskop 40 microscope coupled to a Zeiss Axiocam MRM camera system. The H&E staining tissue sections were examined and photographed by a Nikon ECLIPSE 80i microscope coupled to a Nikon DSFi1 camera system. The acquired pictures were analyzed for myotube diameter as previously described (19) and myofiber cross-sectional area as well as minimum Feret diameter using ImageJ software (NIH).

Ex Vivo Contractile Force Measurement. EDL muscle was dissected from mice immediately after killing. Both proximal and distal tendons were tied using silk sutures in mouse Ringer solution (120 mM NaCl, 4 mM KCl, 2 mM $CaCl_2$, 1 mM $MgSO_4$, 1 mM $MgSO_4$, 1 mM KH_2PO_4, 10 mM glucose, 25 mM $NaHCO_3$, pH 7.2 to 7.4) continuously gassed with 95% O_2/5% CO_2 at 25 °C. The suture tied to the distal tendon was attached onto a fixed hook at the bottom of the bath containing Ringer solution while the suture tied to the proximal tendon was connected to the force transducer (F30, Harvard Apparatus). Contractile properties were assessed by passing a current between two platinum electrodes at supramaximal voltage (PanLab LE 12406, Harvard Apparatus) with pulse and train durations of 0.5 and 250 ms, respectively. After equilibrating in 95% O_2/5% CO_2 gassed Ringer solution at 30 °C for 15 min, muscle length was adjusted to elicit maximum twitch force (optimal length, Lo). The Lo was then measured using a hand-held electronic caliper. Muscle was allowed another 5-min equilibration period. Contractile forces were measured at stimulation frequencies of 1, 5, 10, 20, 40, 60, 80, 120, 150, and 200 Hz every 1 min. After the contractile protocol, EDL muscle was removed from the bath, trimmed of excess connective tissue, blotted dry, and weighed. Muscle weight and Lo was used to estimate the cross-sectional area and normalized forces were expressed as N/cm^2.

Western Blotting. Muscle homogenate and myotube lysate were prepared in ice-cold RIPA buffer containing 50 mM Tris·HCl (pH 7.5), 150 mM NaCl, 2 mM ethylenediaminetetraacetic acid, 1% Nonidet P-40, 0.1% sodium dodecyl sulfate (SDS) and phosphatase/protease inhibitor mixtures. Insoluble tissue or cell debris was removed by centrifugation at 16,000 × *g* for 15 min at 4 °C. The protein concentration in supernatant fraction was determined using the BCA protein assay kit with BSA as a standard. Proteins were separated by sodium dodecyl sulfate–polyacrylamide gel electrophoresis (SDS-PAGE) and transferred to nitrocellulose membranes. After blocking by 5% milk in tris-buffered saline with Tween 20, the membranes were incubated with a primary antibody at 4 °C from 1 h to overnight. Horseradish peroxidase-conjugated secondary antibodies were used to locate the primary antibodies by the enhanced chemiluminescence method. The information and dilutions of all antibodies are listed in *SI Appendix*, Table S1. Optical density of bands detected on the X-ray films was quantified using ImageJ software (NIH) and normalized to GAPDH, α-tubulin, or vinculin except that LC3-II was normalized to LC3-I. Normalized data are expressed in arbitrary units in comparison to controls.

Quantitative PCR. Total RNA was extracted from myotubes or mouse muscle using TRIzol reagent (Thermo Fisher Scientific) and dissolved in diethylpyrocarbonate-treated water. Total RNA (0.5 μg) was reverse transcribed to cDNA using the RevertAid First Strand cDNA Synthesis kit (Thermo Fisher Scientific). Quantitative PCR was performed using the SYBR Green RT-PCR kit (Thermo Fisher Scientific). Sequences of specific primers are Atrogin1/MAFbx, F 5′-CACATTCTCTCCTGGAAGGGC-3′, R 5′-TTGATAAAGTCTTGAGGG GAAAGTG-3′; MuRF1, F 5′-CACGAAGACGAGAAGATCAACATC-3′, R 5′-AGCCC CAAACACCTTGCA-3′; and GAPDH, F 5′-CATGGCCTTCCGTGTTCCTA-3′, R 5′-GCGG CACGTCAGATCCA-3′. Detected levels of target mRNAs were calculated using the ΔΔCt method and normalized to GAPDH in arbitrary units.

Statistical Analysis. Data were analyzed with Student's *t* test, analysis of variance (ANOVA), χ^2 test, or Pearson's correlation coefficient test as appropriate using SigmaStat software (Systat Software). *P* values less than 0.05 were considered statistically significant and indicated by *. Data are presented as means ± SD.

Data, Materials, and Software Availability. All study data are included in the article and/or *SI Appendix*.

ACKNOWLEDGMENTS. This study was supported by grants from the National Institute of Arthritis and Musculoskeletal and Skin Diseases to Y.-P.L. (R01 AR067319 and R01 AR063786).

Author affiliations: [a]Department of Integrative Biology and Pharmacology, University of Texas Health Science Center at Houston, Houston, TX 77030; [b]Department of Molecular Physiology and Biophysics, Baylor College of Medicine, Houston, TX 77030; [c]Geriatric Research, Education, and Clinical Center, VA Puget Sound Health Care System, Seattle, WA98018; [d]Department of Medicine, Division of Gerontology and Geriatric Medicine, University of Washington, Seattle, WA98108; and [e]World Class University Program, Department of Molecular Medicine and Biopharmaceutical Sciences, Graduate School of Convergence Science and Technology and College of Medicine, Seoul National University, Seoul 110-799, Korea

Author contributions: Y.-P.L. designed research; S.G., G.Z., Z.Z., J.Z.Z., Y.Z., G.G.R., and R.S.A.-Z. performed research; L.L., L.A., J.M.G., and Y.T.K. contributed new reagents/analytic tools; S.G. and G.Z. analyzed data; and S.G. and Y.-P.L. wrote the paper.

1. M. Sadeghi *et al.*, Cancer cachexia: Diagnosis, assessment, and treatment. *Crit. Rev. Oncol. Hematol.* **127**, 91–104 (2018).
2. K. Fearon *et al.*, Definition and classification of cancer cachexia: An international consensus. *Lancet Oncol.* **12**, 489–495 (2011).
3. S. Acharyya *et al.*, Dystrophin glycoprotein complex dysfunction: A regulatory link between muscular dystrophy and cancer cachexia. *Cancer Cell* **8**, 421–432 (2005).
4. Y. Wang, J. E. Pessin, Mechanisms for fiber-type specificity of skeletal muscle atrophy. *Curr. Opin. Clin. Nutr. Metab. Care* **16**, 243–250 (2013).
5. Y. P. Li, R. J. Schwartz, I. D. Waddell, B. R. Holloway, M. B. Reid, Skeletal muscle myocytes undergo protein loss and reactive oxygen-mediated NF-kappaB activation in response to tumor necrosis factor alpha. *FASEB J.* **12**, 871–880 (1998).
6. S. H. Lecker, V. Solomon, W. E. Mitch, A. L. Goldberg, Muscle protein breakdown and the critical role of the ubiquitin-proteasome pathway in normal and disease states. *J. Nutr.* **129** (1S, suppl.), 227S–237S (1999).
7. S. Schiaffino, C. Reggiani, Fiber types in mammalian skeletal muscles. *Physiol. Rev.* **91**, 1447–1531 (2011).

8. J. Fielitz *et al.*, Myosin accumulation and striated muscle myopathy result from the loss of muscle RING finger 1 and 3. *J. Clin. Invest.* **117**, 2486–2495 (2007).
9. S. Cohen *et al.*, During muscle atrophy, thick, but not thin, filament components are degraded by MuRF1-dependent ubiquitylation. *J. Cell Biol.* **185**, 1083–1095 (2009).
10. B. A. Clarke *et al.*, The E3 Ligase MuRF1 degrades myosin heavy chain protein in dexamethasone-treated skeletal muscle. *Cell Metab.* **6**, 376–385 (2007).
11. C. Polge *et al.*, Muscle actin is polyubiquitinylated in vitro and in vivo and targeted for breakdown by the E3 ligase MuRF1. *FASEB J.* **25**, 3790–3802 (2011).
12. V. Solomon, S. H. Lecker, A. L. Goldberg, The N-end rule pathway catalyzes a major fraction of the protein degradation in skeletal muscle. *J. Biol. Chem.* **273**, 25216–25222 (1998).
13. V. Solomon, V. Baracos, P. Sarraf, A. L. Goldberg, Rates of ubiquitin conjugation increase when muscles atrophy, largely through activation of the N-end rule pathway. *Proc. Natl. Acad. Sci. U.S.A.* **95**, 12602–12607 (1998).
14. S. H. Lecker *et al.*, Ubiquitin conjugation by the N-end rule pathway and mRNAs for its components increase in muscles of diabetic rats. *J. Clin. Invest.* **104**, 1411–1420 (1999).
15. M. D. Gomes, S. H. Lecker, R. T. Jagoe, A. Navon, A. L. Goldberg, Atrogin-1, a muscle-specific F-box protein highly expressed during muscle atrophy. *Proc. Natl. Acad. Sci. U.S.A.* **98**, 14440–14445 (2001).
16. S. C. Bodine *et al.*, Identification of ubiquitin ligases required for skeletal muscle atrophy. *Science* **294**, 1704–1708 (2001).
17. Y. T. Kwon *et al.*, Female lethality and apoptosis of spermatocytes in mice lacking the UBR2 ubiquitin ligase of the N-end rule pathway. *Mol. Cell. Biol.* **23**, 8255–8271 (2003).
18. K. S. Kwak *et al.*, Regulation of protein catabolism by muscle-specific and cytokine-inducible ubiquitin ligase E3alpha-II during cancer cachexia. *Cancer Res.* **64**, 8193–8198 (2004).
19. G. Zhang *et al.*, Tumor induces muscle wasting in mice through releasing extracellular Hsp70 and Hsp90. *Nat. Commun.* **8**, 589 (2017).
20. S. M. Judge *et al.*, Genome-wide identification of FoxO-dependent gene networks in skeletal muscle during C26 cancer cachexia. *BMC Cancer* **14**, 997 (2014).
21. G. Zhang, R. K. Lin, Y. T. Kwon, Y. P. Li, Signaling mechanism of tumor cell-induced up-regulation of E3 ubiquitin ligase UBR2. *FASEB J.* **27**, 2893–2901 (2013).
22. G. Zhang *et al.*, Weight loss in cancer patients correlates with p38β MAPK activation in skeletal muscle. *Front. Cell Dev. Biol.* **9**, 784424 (2021).
23. A. Narasimhan *et al.*, Profiling of adipose and skeletal muscle in human pancreatic cancer cachexia reveals distinct gene profiles with convergent pathways. *Cancers (Basel)* **13**, 1975 (2021).
24. Z. Liu *et al.*, p38β MAPK mediates ULK1-dependent induction of autophagy in skeletal muscle of tumor-bearing mice. *Cell Stress* **2**, 311–324 (2018).
25. T. K. Sin *et al.*, Cancer-induced muscle wasting requires p38β MAPK activation of p300. *Cancer Res.* **81**, 885–897 (2021).
26. G. Zhang, B. Jin, Y. P. Li, C/EBPβ mediates tumour-induced ubiquitin ligase atrogin1/MAFbx upregulation and muscle wasting. *EMBO J.* **30**, 4323–4335 (2011).
27. F. Pin *et al.*, Growth of ovarian cancer xenografts causes loss of muscle and bone mass: A new model for the study of cancer cachexia. *J. Cachexia Sarcopenia Muscle* **9**, 685–700 (2018).
28. S. Gao, J. A. Carson, Lewis lung carcinoma regulation of mechanical stretch-induced protein synthesis in cultured myotubes. *Am. J. Physiol. Cell Physiol.* **310**, C66–C79 (2016).
29. S. R. Hingorani *et al.*, Trp53R172H and KrasG12D cooperate to promote chromosomal instability and widely metastatic pancreatic ductal adenocarcinoma in mice. *Cancer Cell* **7**, 469–483 (2005).
30. K. Foley *et al.*, Semaphorin 3D autocrine signaling mediates the metastatic role of annexin A2 in pancreatic cancer. *Sci. Signal.* **8**, ra77 (2015).
31. K. A. Michaelis *et al.*, Establishment and characterization of a novel murine model of pancreatic cancer cachexia. *J. Cachexia Sarcopenia Muscle* **8**, 824–838 (2017).
32. T. K. Sin *et al.*, Cancer takes a toll on skeletal muscle by releasing heat shock proteins-an emerging mechanism of cancer-induced cachexia. *Cancers (Basel)* **11**, 1272 (2019).
33. T. Tasaki *et al.*, The substrate recognition domains of the N-end rule pathway. *J. Biol. Chem.* **284**, 1884–1895 (2009).
34. J. S. Thrower, L. Hoffman, M. Rechsteiner, C. M. Pickart, Recognition of the polyubiquitin proteolytic signal. *EMBO J.* **19**, 94–102 (2000).
35. H. Gonen *et al.*, Isolation, characterization, and partial purification of a novel ubiquitin-protein ligase, E3. Targeting of protein substrates via multiple and distinct recognition signals and conjugating enzymes. *J. Biol. Chem.* **271**, 302–310 (1996).
36. P. Bergmann, K. Militzer, P. Schmidt, D. Büttner, Sex differences in age development of a mouse inbred strain: Body composition, adipocyte size and organ weights of liver, heart and muscles. *Lab. Anim.* **29**, 102–109 (1995).
37. V. Smerdu, I. Karsch-Mizrachi, M. Campione, L. Leinwand, S. Schiaffino, Type IIx myosin heavy chain transcripts are expressed in type IIb fibers of human skeletal muscle. *Am. J. Physiol.* **267**, C1723–C1728 (1994).
38. T. K. Sin, J. Z. Zhu, G. Zhang, Y. P. Li, p300 mediates muscle wasting in Lewis lung carcinoma. *Cancer Res.* **79**, 1331–1342 (2019).
39. S. Trappe *et al.*, Skeletal muscle signature of a champion sprint runner. *J. Appl. Physiol. (1985)* **118**, 1460–1466 (2015).
40. J. Zhao *et al.*, FoxO3 coordinately activates protein degradation by the autophagic/lysosomal and proteasomal pathways in atrophying muscle cells. *Cell Metab.* **6**, 472–483 (2007).
41. J. M. Sacheck *et al.*, Rapid disuse and denervation atrophy involve transcriptional changes similar to those of muscle wasting during systemic diseases. *FASEB J.* **21**, 140–155 (2007).
42. T. N. Stitt *et al.*, The IGF-1/PI3K/Akt pathway prevents expression of muscle atrophy-induced ubiquitin ligases by inhibiting FOXO transcription factors. *Mol. Cell* **14**, 395–403 (2004).
43. K. R. Bohnert *et al.*, Inhibition of ER stress and unfolding protein response pathways causes skeletal muscle wasting during cancer cachexia. *FASEB J.* **30**, 3053–3068 (2016).
44. F. Penna, F. M. Baccino, P. Costelli, Coming back: Autophagy in cachexia. *Curr. Opin. Clin. Nutr. Metab. Care* **17**, 241–246 (2014).
45. J. A. Carson, J. P. Hardee, B. N. VanderVeen, The emerging role of skeletal muscle oxidative metabolism as a biological target and cellular regulator of cancer-induced muscle wasting. *Semin. Cell Dev. Biol.* **54**, 53–67 (2016).
46. A. Roy, A. Kumar, ER stress and unfolded protein response in cancer cachexia. *Cancers (Basel)* **11**, 1929 (2019).
47. A. Varshavsky, The N-end rule pathway and regulation by proteolysis. *Protein Sci.* **20**, 1298–1345 (2011).
48. R. T. Jagoe, A. L. Goldberg, What do we really know about the ubiquitin-proteasome pathway in muscle atrophy? *Curr. Opin. Clin. Nutr. Metab. Care* **4**, 183–190 (2001).
49. C. D'Orlando *et al.*, Gastric cancer does not affect the expression of atrophy-related genes in human skeletal muscle. *Muscle Nerve* **49**, 528–533 (2014).
50. I. J. Gallagher *et al.*, Suppression of skeletal muscle turnover in cancer cachexia: Evidence from the transcriptome in sequential human muscle biopsies. *Clin. Cancer Res.* **18**, 2817–2827 (2012).
51. C. M. Op den Kamp *et al.*, Nuclear transcription factor κ B activation and protein turnover adaptations in skeletal muscle of patients with progressive stages of lung cancer cachexia. *Am. J. Clin. Nutr.* **98**, 738–748 (2013).
52. N. A. Stephens *et al.*, Using transcriptomics to identify and validate novel biomarkers of human skeletal muscle cancer cachexia. *Genome Med.* **2**, 1 (2010).
53. N. Johns *et al.*, Clinical classification of cancer cachexia: Phenotypic correlates in human skeletal muscle. *PLoS One* **9**, e83618 (2014).
54. A. M. Dingemans, J. de Vos-Geelen, R. Langen, A. M. Schols, Phase II drugs that are currently in development for the treatment of cachexia. *Expert Opin. Investig. Drugs* **23**, 1655–1669 (2014).
55. M. I. Ramage, R. J. E. Skipworth, The relationship between muscle mass and function in cancer cachexia: Smoke and mirrors? *Curr. Opin. Support. Palliat. Care* **12**, 439–444 (2018).
56. S. M. Advani, P. G. Advani, H. M. VonVille, S. H. Jafri, Pharmacological management of cachexia in adult cancer patients: A systematic review of clinical trials. *BMC Cancer* **18**, 1174 (2018).
57. G. E. Truett *et al.*, Preparation of PCR-quality mouse genomic DNA with hot sodium hydroxide and tris (HotSHOT). *Biotechniques* **29**, 52–54 (2000).
58. G. Zhang, Y. P. Li, p38β MAPK upregulates atrogin1/MAFbx by specific phosphorylation of C/EBPβ. *Skelet. Muscle* **2**, 20 (2012).